TRƯỜNG ĐẠI HỌC SÀI GÒN
TẠP CHÍ KHOA HỌC
ĐẠI HỌC SÀI GÒN
ISSN 1859-3208
e-ISSN 3093-3056
Số 97, Tập 01/2025

SAIGON UNIVERSITY
SCIENTIFIC JOURNAL
OF SAIGON UNIVERSITY
No. 97, Vol 01/2025

Email: tcdhsg@sgu.edu.vn ; Website: http://sj.sgu.edu.vn/

S-SCHEME ZnO-WO_3 HETEROJUNCTION FOR BOOSTING SYNTHETIC DYE PHOTODEGRADATION IN AQUEOUS SOLUTIONS

Cấu trúc dị thể S-Scheme ZnO-WO_3 nhằm tăng cường quang phân hủy thuốc nhuộm tổng hợp trong dung dịch nước

Le Thi Thanh Thuy[(1)], Pham Thi Giang Anh[(1)], Pham Thi Thanh Hien[(1)]
Tran Dinh Trinh[(2)], Pham Thi Thuy[(1)*]

[(1)]Saigon University
[(2)]VNU University of Science

ABSTRACT

In this study, a ZnO-WO_3 heterojunction was synthesized from Zn^{2+} and W^{6+} precursors using sol-gel and calcination methods. The structural, chemical, and optical properties of the resulting materials were characterized by a range of techniques including XRD, UV-Vis, SEM/TEM, EDX, FT-IR, and BET. The synthesized ZnO-WO_3 materials were subsequently tested for their photocatalytic activity in the degradation of synthetic dyes under visible light. The effects of varying W/Zn molar ratios and contaminant concentrations on photocatalytic performance were investigated. The formation of the ZnO-WO_3 heterojunction reduced the band gap to 2.84 eV, enabling efficient photocatalysis under visible light. The ZnO-WO_3 heterojunction exhibited 2-4 times higher photodegradation efficiency for methylene blue (MB) compared to pure ZnO and WO_3. This enhanced performance was attributed to the formation of an S-scheme heterojunction, which effectively suppressed charge carrier recombination. The MB degradation process followed pseudo-first-order kinetics, and the ZnO-WO_3 photocatalyst demonstrated excellent stability and reusability throughout multiple cycles.

Keywords: *Visible light driven-photocatalysts, heterojunction, ZnO, synthetic dyes, improvement, reusability.*

TÓM TẮT

Trong nghiên cứu này, dị thể ZnO-WO_3 đã được tổng hợp từ các tiền chất Zn^{2+} và W^{6+} thông qua phương pháp sol-gel kết hợp với nung kết. Các đặc tính cấu trúc, hóa học và quang học của vật liệu thu được đã được khảo sát bằng nhiều kỹ thuật khác nhau như XRD, UV-Vis, SEM/TEM, EDX, FT-IR và BET. Vật liệu ZnO-WO_3 tổng hợp sau đó được đánh giá hoạt tính quang xúc tác trong quá trình phân hủy các thuốc nhuộm tổng hợp dưới ánh sáng khả kiến. Ảnh hưởng của tỷ lệ mol W/Zn và nồng độ chất ô nhiễm đến hiệu suất quang xúc tác cũng được nghiên cứu. Sự hình thành dị thể ZnO-WO_3 giúp giảm năng lượng vùng cấm xuống còn 2,84 eV, cho phép xúc tác hiệu quả dưới ánh sáng khả kiến. Dị thể ZnO-WO_3 thể hiện hiệu suất phân hủy methylene blue (MB) cao hơn gấp 2-4 lần so với ZnO và WO_3 tinh khiết. Hiệu suất vượt trội này được cho là nhờ vào sự hình thành cấu trúc dị thể theo cơ chế S-scheme, giúp ức chế hiệu quả sự tái kết hợp của các cặp điện tử–lỗ trống. Quá trình phân hủy MB tuân theo động học bậc một giả, và chất xúc tác ZnO–WO_3 thể hiện độ bền và khả năng tái sử dụng tuyệt vời qua nhiều chu kỳ.

Từ khóa: *Quang xúc tác kích hoạt bởi ánh sáng khả kiến, dị thể bán dẫn, ZnO, thuốc nhuộm tổng hợp, cải thiện hiệu suất, tái sử dụng.*

[*]Corresponding author: phamthithuy@sgu.edu.vn

1. Introduction

Each year, approximately 280,000 tons of dyes are released into the environment as a result of industrial activities [1,2]. Dyes are widely used in industries such as printing, paper production [3-5], textiles [6,7], pharmaceuticals [8], and more. However, these dyes are typically non-biodegradable and highly toxic to both the environment and human health [9]. Moreover, dye pollution disrupts the growth of aquatic plants [10]. Traditional wastewater treatment methods are often ineffective at degrading synthetic dyes [11], leaving behind toxic residues in water bodies that continue to harm the environment [12]. Among various water pollution control techniques, photocatalysis has gained significant attention due to its high efficiency, simplicity, regeneration potential, and ease of use in the degradation of organic pollutants [13,14,15].

Along with outstanding advantages, photocatalytic process can also completely oxidize organic contaminants to form CO_2 and H_2O [13]. Photocatalysts such as TiO_2, ZnO, CdS, GaP, and ZnS have shown remarkable efficiency in breaking down organic pollutants, transforming them into biodegradable substances and mineralizing them into CO_2 and H_2O [13,16]. ZnO, in particular, is an n-type semiconductor with a band gap of approximately 3.3 eV, which makes it a promising alternative to TiO_2 for contaminant degradation [17,18]. Known for its excellent optical, mechanical, and electrical properties, ZnO is also widely recommended for antibacterial applications [19]. However, its high band gap energy (Eg) limits its effectiveness under visible light, restricting its environmental applications. Another challenge is the high recombination rate of photogenerated electron-hole pairs, which reduces the efficiency of the photocatalytic process [20]. WO_3 possesses several desirable properties for photocatalysis [21], but its standalone performance also has limitations [22]. To overcome these drawbacks, various strategies have been explored, including doping with metals or non-metals [23,24], hybridizing with nanomaterials like g-C_3N_4 or graphene [25,26], and forming heterojunctions with other metal oxide semiconductors [27]. Notably, the combination withmetal oxide semiconductors offers several advantages for enhancing photocatalytic activity [28,29], enabling photogenerated electrons and holes to fully exploit their potential [30]. Therefore, in this study, we developed a S-scheme photocatalyst based on ZnO-WO_3 heterojunction to take full advantage of the excellent properties that bring high efficiency in dye photodegradation. In this study, ZnO-WO_3 materials were produced by sol-gel and calcination methods. The produced materials' physical and chemical properties were characterized using SEM, TEM, EDX, BET, XRD, FT-IR, and UV-Vis methods. They were then applied to study the photodegradation of MB in aqueous solutions by visible light.

2. Experimental

2.1. Chemical

Oxalic acid ($C_2H_2O_4.2H_2O$ 99.5%), zinc nitrate ($Zn(NO_3)_2.6H_2O$ 99%), ethyl alcohol (C_2H_5OH 99.7%, PA), nitric acid (HNO_3 68%), sodium tungstate dihydrate ($Na_2WO_4.2H_2O$, Merck), methylene blue ($C_{16}H_{18}ClN_3S.3H_2O$).

2.2. Synthesis of ZnO-WO_3 nanocomposites

Solution A was prepared by slowly pouring 200 mL of 0.6 M $H_2C_2O_4$ solution into 200 mL of 0.4 M $Zn(NO_3)_2$ solution. Solution B was prepared by mixing 35 mL of anhydrous C_2H_5OH, 1 mL of HNO_3, and

2 mL of deionized (DI) water. Next, an appropriate amount (0.8, 1.0, 1.2, 1.4, or 1.6 g) of $Na_2WO_4.2H_2O$ was added to the resulting mixture to get desired $(W/Zn)_x$ molar ratios, in which x values ranged from 0.06 to 0.12. Solution B was then stirred thoroughly using a magnetic stirrer until complete dissolution was achieved. Next, solution A was dropwise added into solution B. The resulting mixture was vigorously stirred on a magnetic stirrer at room temperature for 2 h. This process resulted in the formation of a light blue sol which was then left to age into a gel at room temperature for 2 days. Subsequently, the gel was subjected to be drying at 100 °C for 3 h, followed by a calcination at 425 °C for 3 h to obtain the $ZnO\text{-}xWO_3$ material.

Regarding the synthesis of ZnO semiconductor, solution A was stirred until the formation of precipitation. The reaction was kept at room temperature for 2h, then the precipitate was separated and collected by centrifuge at 3,000 rpm, filtration and washing with DI water. The obtained precipitate was then dried at 100 °C for 3 h, then calcined at 450 °C for 4 h to get ZnO nanoparticles. To synthesize WO_3 nanoparticle, solution B was stirred at room temperature for 2h until a transparent sol was achieved. The sol was aged for 2 days to form a gel which was subsequently dried at 100 °C for 3 h and further calcined at 450 °C for 4 h to obtain WO_3 material.

2.3. Photocatalytic activity experiments

Photocatalytic activity was assessed by the decomposition of 20 mg/L MB in solutions using a catalyst dosage of 2.5 g/L. The mixture was stirred in dark for 60 min to achieve absorption equilibrium, and subsequently irradiated by a LED bulb (40W, 220V) emitting light wavelengths spanning from 400 nm to 700 nm. Spectrophotometric analysis was employed to track the change in MB concentration as a function of time as presented in the subsequent section.

2.4. Characterization and analytical methods

The crystalline structure of the materials was determined using X-ray diffraction (XRD) method (D8 - Advance 5005). Elemental composition of the samples was identified through Energy-Dispersive X-ray Spectroscopy (EDX) (JEOL-JSM 6490). Surface morphology, boundaries, and particle size were examined using Scanning Electron Microscopy (SEM) (Hitachi S4800) and Transmission Electron Microscopy (TEM) (JEOL JEM-1010 Electron Microscope). Optical properties of the catalyst systems were characterized by UV-Visible Diffuse Reflectance Spectroscopy (UV-Vis DRS) (Tasco-V670 photospectrometer). Porosity and specific surface area of the samples were assessed using the BET method, measured by a NOVAtouch LX4, Quantachrome Instrument. Functional groups were identified using Fourier Transform Infrared Spectroscopy (FT-IR), model JASCO 4600. The concentration of MB was determined using spectrophotometric analysis at a wavelength of 663 nm (UV-Vis Hitachi U-5100, Japan).

3. Results and Discussion

3.1. Features of the materials' structure

The X-ray diffraction pattern of WO_3 (**Fig. 1**) shows that characteristic signals corresponding to the main reflection of WO_3 were detected at 23.11°, 23.67°, 24.23°, and 26.7°, corresponding to (002), (020), (200) and (120) crystal planes. These results are consistent with JCPDS card No.83-0950 and those in earlier reports [31,32]. On the XRD diagram of pristine ZnO, there was the appearance of

diffraction characteristic peaks of the hexagonal wurtzite structure of ZnO at 2θ = 31.87°, 34.36°, 36.25°, 47.92°, 56.62°, 62.89°, 68.08°, which corresponded to the plane family (100); (002); (101); (102); (110); (103); (112). These obtained results are in accordance with previous reports [33-35]. The X-ray diffraction (XRD) findings of the ZnO-WO_3 composite material reveal distinct peaks associated with ZnO and WO materials, signifying the effective combination of these individuals to form a ZnO-WO_3 photocatalytic material. It is noted that due to the low peak intensity of WO3 and the small proportion of WO_3 doped, characteristic peaks of WO_3 were not significantly in the ZnO-WO_3 nanocomposites (**Fig. 1a**). EDX analyses of WO_3, ZnO, and ZnO-WO_3 revealed a clear presence of W and O elements in WO_3 sample, Zn and O elements in ZnO sample, and W, Zn, and O elements in ZnO-WO_3 nanocomposites, which did not present any significant impurities (**Fig. 1b**). EDX mapping of the elements in ZnO (**Fig. 1c-e**), WO_3 (**Fig. 1f-h**) and ZnO-WO_3 (**Fig. 1i-m**) showed very good elemental distribution in the examined samples, suggesting a successful creation of ZnO-WO_3 nanocomposite. The scanning electron microscope (SEM) analysis revealed that the sample exhibits a reasonably consistent porous grain structure and a relatively uniform surface (**Fig. 1o**). Meanwhile, transmission electron microscope (TEM) image demonstrated the formation of ZnO-WO_3 composites with an average particle size of approximately 19 nm (**Fig. 1p**). Interestingly, this particle size estimation closely matched the calculations based on the XRD data using the Debye-Scherrer formula. These findings collectively affirmed that the ZnO-WO_3 nanocomposites obtained in this study was indeed in the nano-sized range.

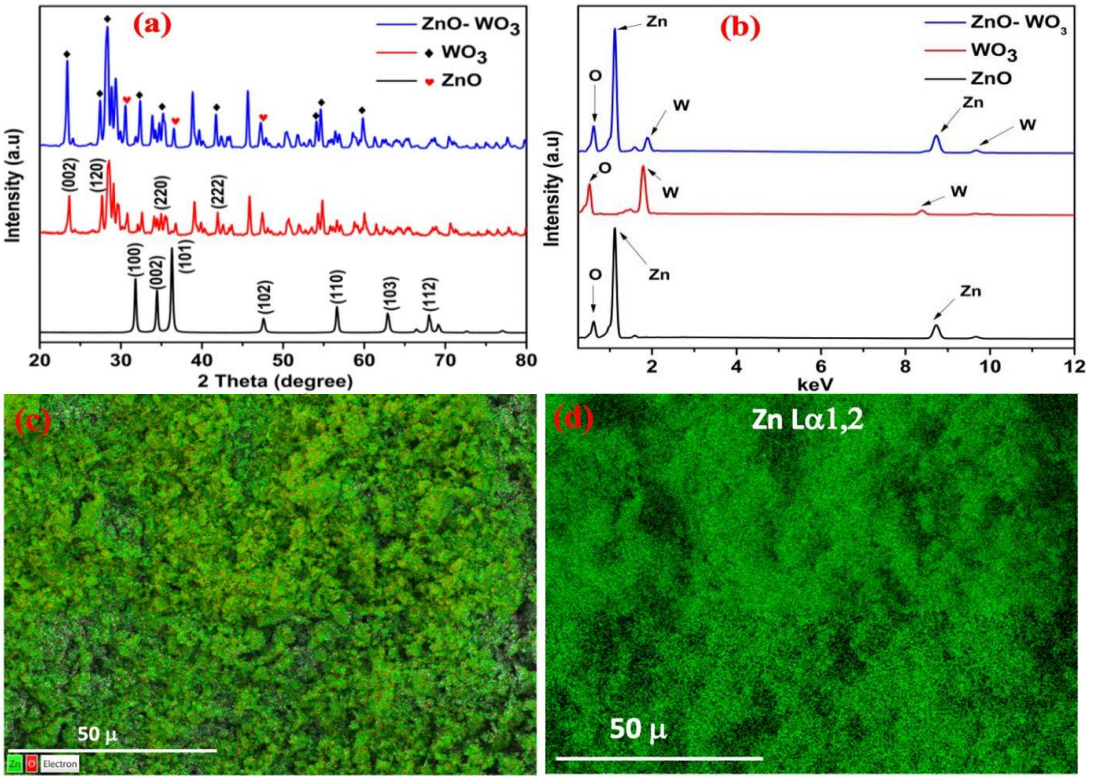

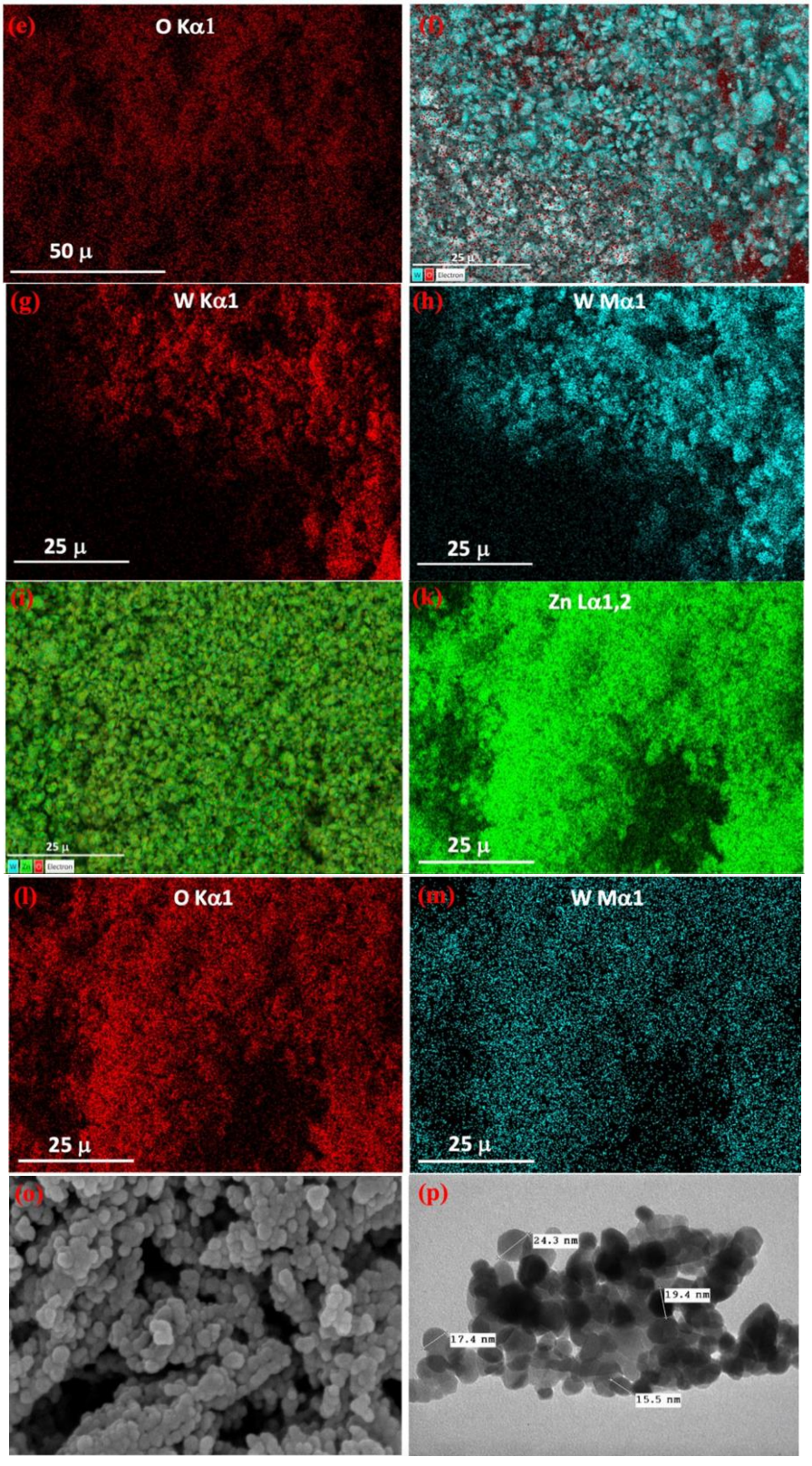

Fig. 1. (a) XRD patterns, (b) EDX analyses, EDX mappings of ZnO (c – e), WO_3 (f – h), and ZnO-WO_3 materials (i – m), (o) SEM, and (p) TEM images of ZnO-WO_3 sample.

FT-IR results (**Fig 2a**) indicated that the vibration peak at 670 cm^{-1} was associated with the O-W-O bond of the WO_3 crystal [36], while the characteristic peak at 436 cm^{-1} was attributed to the stretching vibration of the Zn-O bond of ZnO lattice [37]. The presence of Zn-O and O-W-O bonds in the ZnO-WO_3 confirmed successful synthesis of ZnO-WO_3 photocatalysts. The UV-Vis absorption spectrum and Tauc plot presented in **Fig. 2b,c** indicated a notable reduction in the band gap energy (Eg) of ZnO when it was combined with WO nanoparticles. Specifically, the calculated Eg of ZnO-WO_3 was 2.84 eV significantly reduced in comparison to pristine ZnO (3.32 eV) which was in greement with previous reports [38-39]. ZnO-WO_3 samples were therefore visible light responsive photocatalysts. This reduction in band gap energy might be attributed to the doping of W into the crystal lattice of ZnO, and/or formation of a heterojunction between ZnO and WO_3. The heterojunction can also mitigate the recombination rate of photogenerated electrons and holes [31,40]. This enhancement is expected to significantly boost the catalytic activity of the material. WO_3 exhibited an Eg of about 2.2 eV, suggesting a visible light driven photocatalyst (**Fig. 2c**). The obtained results are comparable with previous reports [31,41,42]. Vu et al. [31] and Hasija et al. [41] reported that Eg values of WO_3 nanomaterials were about 2.6 eV while Verma et al. [42] revealed that those values varied from about 2.0 eV to 2.4 eV according to synthesis temperature.

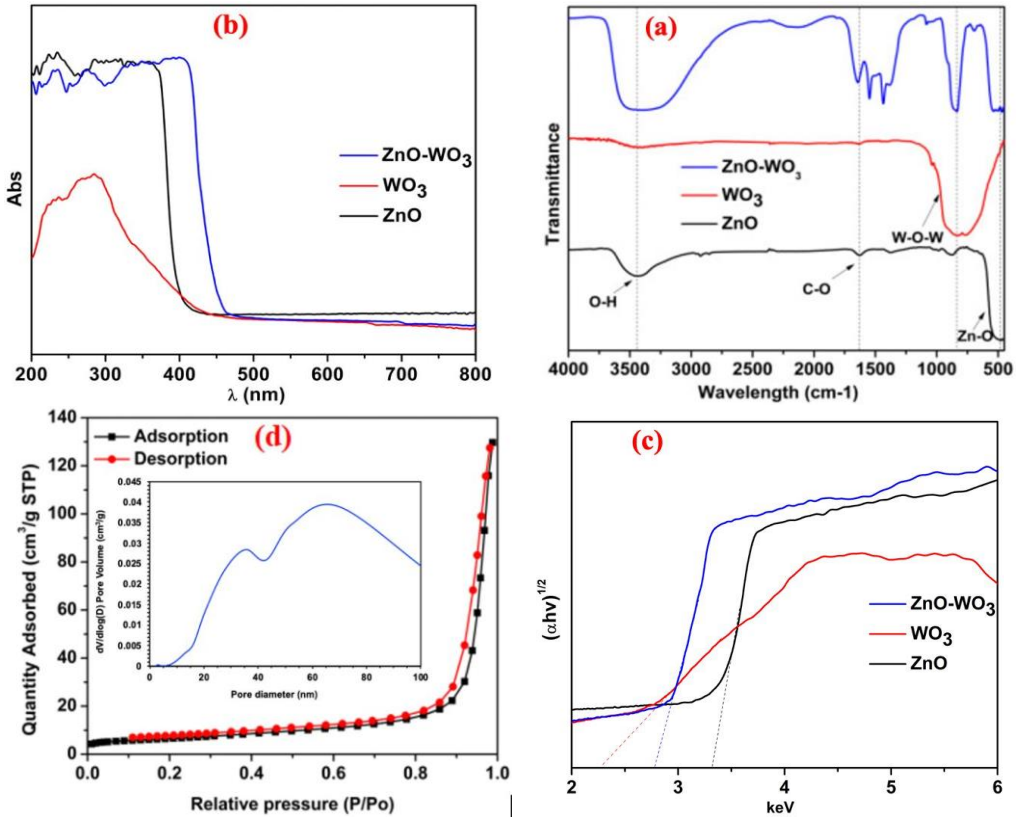

Fig. 2. (a) FT-IR, (b) UV-Vis spectra, (c) Tauc plot of WO_3 and ZnO-WO_3 samples, and (d) N_2 adsorption-desorption isotherms of ZnO-WO_3 samples.

As depicted in **Fig. 2d**, the N_2 adsorption-desorption isotherm conformed to the type IV isotherm and H3 hysteresis loop, as per IUPAC classification [43-45]. This indicates that the ZnO-WO_3 heterojunction was porous materials, with a surface area of 42.53 (m^2/g) and a monomodal pore-size distribution of about 50 nm in diameter. Characterized by porous material, ZnO-WO_3 heterojunction also played an important role in adsorbing and retaining highly reactive organic molecules on its surface. This characteristic would facilitate the catalytic decomposition of organic substances in water.

3.2. Photocatalytic performance of the synthesized materials

3.2.1. Absorption equilibrium and comparison of the photocatalytic performance between synthesized materials

To examine the adsorption capacity of ZnO-WO_3 sample and equilibrium time of MB adsorption process, the ratio of MB concentration at time t (C_t) and initial concentration of MB (C_0) was plotted vs time during the MB adsorption process in dark. It is found that that the adsorption process quickly occurred at the beginning. Subsequently, as the reaction time continued to increase, the adsorption capacity remained nearly constant, indicating that the adsorption process had reached equilibrium at approximately 60 min (**Fig. 3a**). The rapid adsorption of MB during the initial contact can be attributed to the efficient mass transfer of MB molecules, facilitating the access to the ZnO-WO_3's surface. However, the adsorption capacity of the MB remained stable after 60 min, possibly indicating that the saturation of active sites and the limited availability of functional groups on ZnO-WO_3's surface. Thus, 60 min in the dark were chosen prior to conducting the photocatalytic degradation process.

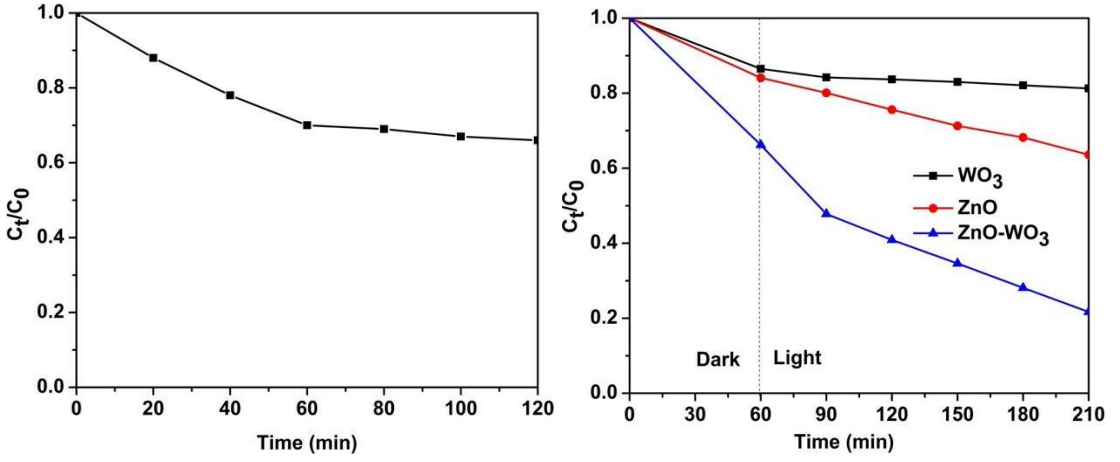

Fig. 3. (a) MB adsorption equilibrium on ZnO-WO_3 sample, and (b) comparison of MB degradation by visible light catalyzed by WO_3, ZnO, and ZnO-WO_3 materials.

The obtained results demonstrate that MB decomposition efficiency under visible light irradiation was significantly enhanced when ZnO photocatalyst was combined with WO_3 semiconductor (**Fig. 3b**). After 210 min of reaction time, the modified

ZnO sample achieved a MB decomposition efficiency of about 80% compared to about 38% for pristine ZnO and only ~18% for sole WO_3. This enhancement can be attributed to i) hybridization of WO_3 oxide with ZnO would create a S-scheme function between WO_3 and ZnO, facilitating electron transfer and prolonging the retention time of photogenerated electrons; ii) doping of W element into ZnO lattice, leading to a decline in Eg of ZnO and therefore the latter expanded its active range from ultraviolet to visible light region. It is noted that, to better understand the level of W doping into ZnO lattice X-ray photoelectron spectroscopy (XPS) analyses should be conducted while the charge carrier recombination restriction by internal electric field formed between WO_3 and ZnO should be analyzed by charge density analysis as well as other electrochemical measurements [46].

3.2.2. Impact of W content and MB concentration on photocatalytic performance of ZnO-WO_3

All ZnO-WO_3 samples containing the W component at different ratios exhibited XRD characteristic peaks of both pristine ZnO and WO_3 (**Fig. 4a**). When the proportion of W increased (W/Zn molar ratio > 0.11), the sharpness of the ZnO diffraction pattern diminished due to a decline in ZnO proportion in the sample. **Fig. 4b** demonstrate that as the amount of W in the sample increased (W:Zn molar ratio from 0.06 to 0.075), the photocatalytic efficiency also increased from about 41.5% to 78.3% after 210 min of reaction. However, when the doping ratio of W exceeds 0.075, the photocatalytic efficiency started to decline to 58% for a W/Zn molar ratio = 0.11.

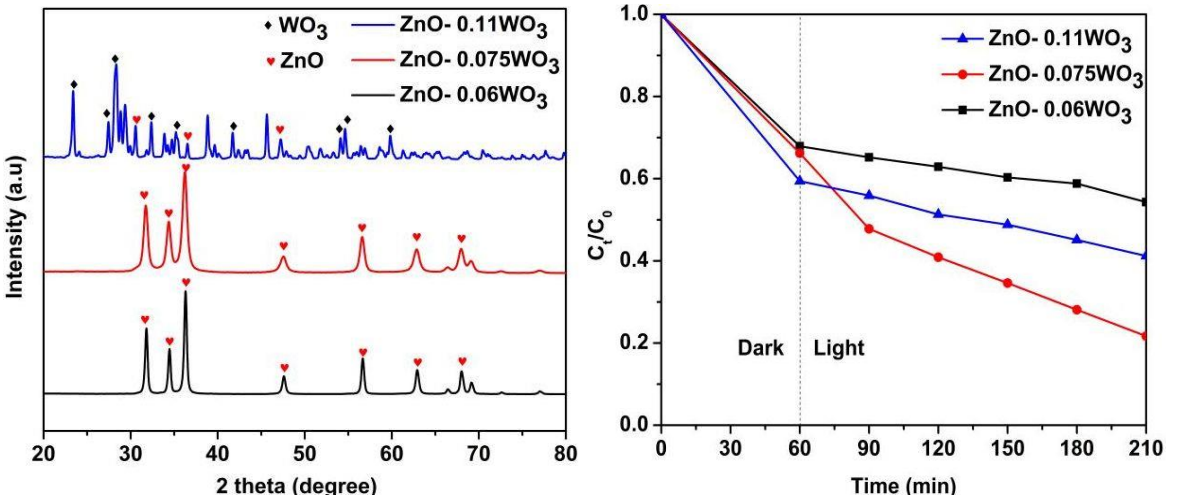

Fig. 4. (a) XRD of ZnO-WO_3 sample with different W:Zn molar ratios, and (b) MB photodegradation by visible light catalyzed by ZnO-xWO_3 heterojunction.

This phenomenon can be explained by the fact that when the tungsten content in the sample is low, the formation of efficient heterojunction between WO_3 and ZnO is limited. When the W^{6+} ions concentration increased the surface barrier became more significant, narrowing the space charge region; hence efficiently

separating charge carriers by more important internal electric field. However, when the W^{6+} ions concentration increased further, the depth of light penetrated into ZnO structure could significantly surpass the layer of space charge, leading to higher recombination of charge carriers [47]. Therefore, a W:Zn molar ratio of 0.075 was optimal and selected for studying the MB photocatalytic degradation.

The first-order kinetics model was applied to experimental data obtained from the photodegradation of MB solutions ranging from 10 mg/L to 80 mg/L. The equation is given as follows [48]:

$$\ln\left(\frac{C}{C_0}\right) = -kt \quad (1)$$

where C_0 (mg/L) and C_t (mg/L) are respectively concentration of MB at initial time (t=0) and a given time (t). k is the rate constant (min^{-1}). The impact of MB initial concentration on photocatalytic performance of ZnO-WO_3 heterojunction system shows that the degradation process well followed the pseudo-1st-kinetics model, with a coefficient of determination ranging from 0.9876 to 0.9965 for a concentration range of 10-80 mg/L (**Fig. 5a**). When MB initial concentration increased from 10 mg/L to 20 mg/L the rate constant (k) augmented from 0.066 min^{-1} to reach a maximum value of 0.0071 min^{-1}. However, k gradually declined to 0.0032 min^{-1} when MB concentration increased from 20 mg/L to 80 mg/L (**Fig. 5a**).

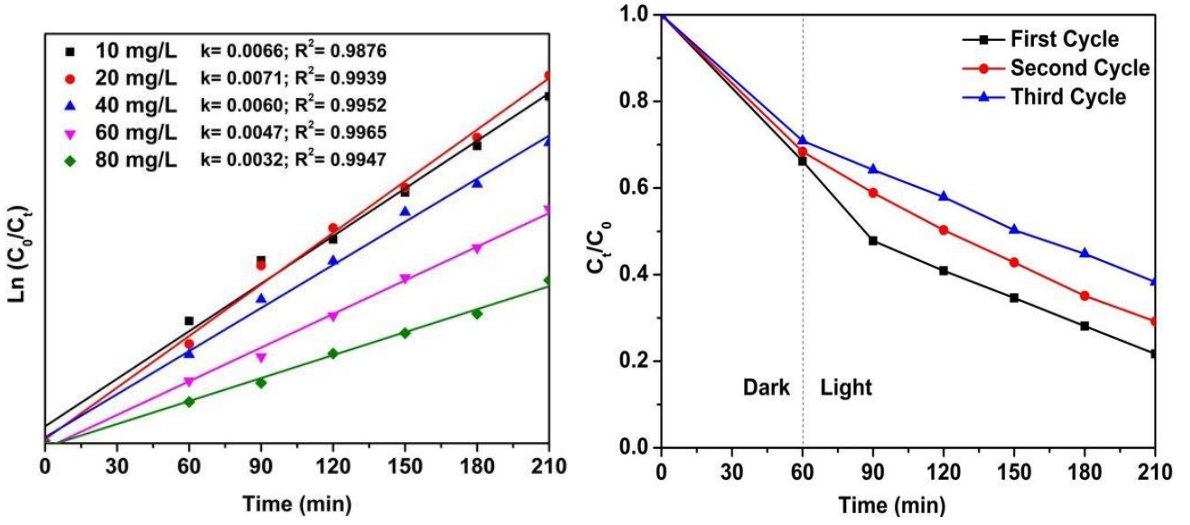

Figure 5. (a) First-order kinetic model applied to the MB photoatalytic degradation process, and (b) Photocatalytic activity of ZnO-WO_3 catalyst at different usage cycles.

This could be attributed to low available contaminant molecules ready for the photodegradation process when MB concentration was low whereas high concentration led to restriction of incident light to surface of the catalytic system for the photocatalytic reaction to occur [32,49].

Table 1. Comparison of photocatalytic performance of different photocatalytic system regarding MB decomposition in aqueous solutions under visible light irradiation.

Material	MB dye conc. (mg/L)	Degradation efficiency (%)	Duration (min)	Reference
$BiVO_4$	5.0	81.0	240	[50]
$BiFeO_3$-$GdFeO_3$	10.0	56.0	120	[51]
ZnO-BiOBr	10.0	42.0	240	[52]
ZnO-MoS_2	3.2	75.0	300	[53]
$MnTiO_3$/TiO_2	32.0	75.0	240	[54]
TiO_2 films	5.0	42.0	300	[55]
$Bi_2VO_{5.5}$	5.0	82.0	240	[56]
ZnO-WO_3	20.0	80.0	210	This work

The comparison of MB photodegradation catalyzed by different photocatalysis is shown in **Table 1**. Generally, the results obtained in this research are comparable to better than others. About 80% of 20 mg/L MB were decomposed after 210 min in the current work, while this was 81% for 5 mg/L MB after 240 min of reaction time and catalyzed by $BiVO_4$ photocatalyst, which was reported by Kumar et al. [50]. In another work, Subramanian et al. [51] found that $BiFeO_3$-$GdFeO_3$ photocatalytic system could help to decompose 56% of 10 mg/L MB after 120 min. Similarly, Geng et al. [52] revealed that 42% of 10 mg/L MB were decomposed by visible light with the aid of ZnO-BiOBr photocatalytic system after 240 min while Benavente et al. [53] found 75% of 3.2 mg/L MB after 300 min with the support of ZnO-MoS_2 photocatalytic system (**Table 1**).

3.2.3. Mechanism proposal, and catalyst recovery and reusability.

As presented previously in the current work, the ZnO-WO_3 heterojunction exhibited an Eg of 2.84 eV, while WO_3 had an Eg of 2.2 eV. Previous studies reported ZnO with an Eg of ~3.30 eV [32, 57]. As Zn^{2+} (ion radius, 0.074 nm) has a slightly larger ionic radius than W^{6+} (ion radius, 0.064 nm), W^{6+} ions could be doped into the ZnO lattice by replacing Zn^{2+} ions, reducing Eg due to structural defects, oxygen deficiencies, and impurities [47, 58]. In addition, W^{6+} doping in ZnO also acts as a charge trap, slowing carrier recombination and enhancing charge transfer between ZnO and WO_3 [47]. This restriction may establish an S-scheme photocatalytic system, where electrons from the CB of WO_3 migrate to the VB of W-doped ZnO. As a result, photoinduced electrons at the CB of W-doped ZnO would react with dissolved oxygen molecules to generate $\bullet O_2^-$, then HO• according to Eq. (2-5) while h^+ at the VB of WO_3 (more positive than redox potential of HO•/H_2O = 2.7 V) would react with H_2O molecule to form HO• as presented in

Eq. (6-7). Finally, HO• photogenerated will degrade MB molecules into intermediates, then CO_2 and H_2O molecules (Eq. 8 and **Fig. 6**).

Generation of HO• and O_2^{-}• at the CB of ZnO semiconductor:.

$$e^- + O_2 \rightarrow \bullet O_2^- \quad (2)$$

$$\bullet O_2^- + H^+ \rightarrow HO_2\bullet \quad (3)$$

$$2HO_2\bullet \rightarrow H_2O_2 + O_2 \quad (4)$$

$$e^- + H_2O_2 \rightarrow HO\bullet + HO^- \quad (5)$$

Generation of HO• at the VB of WO_3 semiconductor

$$h^+ + H_2O \rightarrow HO\bullet + H^+ \quad (6)$$

$$h^+ + HO^- \rightarrow HO\bullet \quad (7)$$

Contaminant degradation

$$MB + HO\bullet \rightarrow \text{Intermediates} \rightarrow CO_2 + H_2O \quad (8)$$

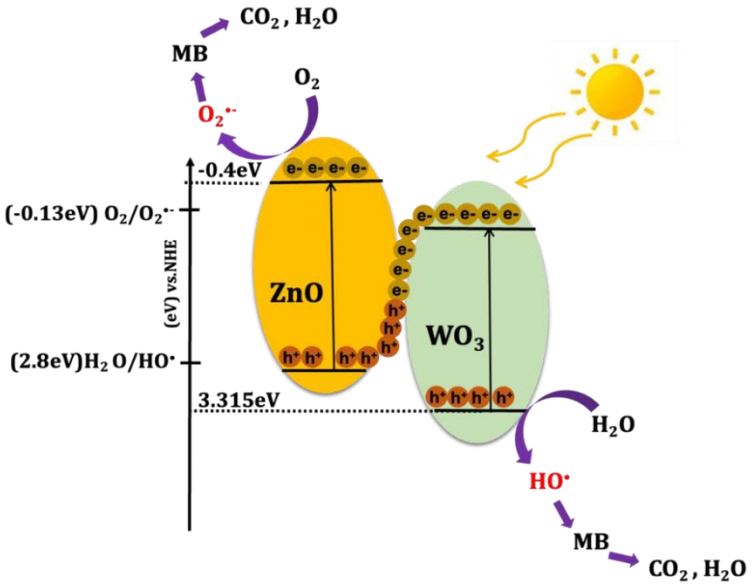

Fig. 6. Mechanism proposal for MB photodegradation in solutions

The reusability of the catalyst is an important factor for practical applications. After the degradation of MB, ZnO-WO_3 was merely separated from the solution by filtration with a Whatman filter paper (pore size of 0.45 µm) and a straightforward rinse with deionized (DI) water. The photocatalyst was subsequently died in an oven at 60 °C for 24 h then kept in a desiccator for subsequent cycles of MB photodegradation experiments. The findings indicated that after three cycles of use, the photocatalyst maintained commendable activity. Its capability to decompose MB remains highly efficient, with a retention of approximately 60% efficiency. These research outcomes

demonstrated the ZnO-WO_3 catalyst's very good durability as a photocatalytic material, rendering it economically viable and well-suited for practical applications.

4. Conclusion

ZnO-WO_3 heterojunction was successfully synthesized with high purity by sol-gel method coupled with calcination process. ZnO-WO_3 nanocomposite exhibited an average particle size of approximately 19 nm, with confirmed compositions of both WO_3 and ZnO semiconductors, and an Eg of 2.84 eV suitable for visible light region. The incorporation of an optimal proportion of W into ZnO lattice and the combination of WO_3 with ZnO were proved to be effective in reducing band gap energy while the formation of a S-scheme heterojunction between ZnO may result in retarding charge carrier recombination. These synergic effects led to a significant enhancement of the photocatalytic performance. W:Zn molar ratio of 0.075 was optimal for producing a ZnO-WO_3 heterojunction with the best photocatalytic performance which was mainly controlled by doping level of W into ZnO structure, space charge region and light penetration depth into ZnO structure.

About 80% of 20 mg/L MB were degraded with the aid of ZnO-WO_3 heterojunction photocatalyst after 210 min, which was more than two times and four times higher than pristine ZnO and WO_3, respectively. The MB photodegradation process respected well the pseudo-1st-order kinetics, with the coefficient (R^2) varied from 0.9876 to 0.9965 for MB concentration sranging from 10 mg/L to 80 mg/L. The ZnO-WO_3 photocatalytic system also presented a very good stability and reusability for MB photodegradation by visible light. The results on MB photodegradation catalyzed by ZnO-WO_3 heterojunction in the current research were comparable to better than several photocatalytic systems reported previously. This study introduces a novel approach to produce ZnO-WO_3 nanocomposite with high photocatalytic performance for the decomposition of toxic organic contaminants by visible light.

Data availability statement

All data that support the findings of this study are included within the article (and any supplementary files).

Disclosure Statement

The author(s) declare that there are no potential conflicts of interest.

Acknowledgement

This work is a part of the research project **CSA2024-09** funded by Saigon University.

REFERENCES

[1] Mohammad A. Al-Ghouti & Samah S. Dib, (2020, Jan.). "Utilization of nano-olive stones in environmental remediation of methylene blue from water", *Journal of Environmental Health Science and Engineering*. 18, pp. 63–77. Available: https://doi.org/10.1007/s40201-019-00438-y.

[2] Anthea Marika G. Domacena, Christian Laurence E. Aquino, Mary Donnabelle L. Balela, (2020). "Photo-Fenton Degradation of Methyl Orange Using Hematite (α-Fe_2O_3) of Various Morphologies", *Materialstoday proceedings*. 22(2), pp. 248-254. Available: https://doi.org/10.1016/j.matpr.2019.08.095.

[3] Sonu Kumar, R.D. Kaushik, L.P. Purohit, (2021, April.). "Novel ZnO tetrapod-reduced graphene oxide nanocomposites for enhanced photocatalytic degradation of phenolic compounds and MB dye", *Journal of Molecular Liquids*. 327, pp. 114814. Available: https://doi.org/10.1016/j.molliq.2020.114814.

[4] Neha Tavker, Manu Sharma, (2020, Feb.). "Designing of waste fruit peels extracted cellulose supported molybdenum sulfide nanostructures for photocatalytic degradation of RhB dye and industrial effluent", *Journal of Environmental Management*. 255, pp. 109906. Available: https://doi.org/10.1016/j.jenvman.2019.109906.

[5] Muhammad Usman, Adeel Ahmed, Bing Yu, Qiaohong Peng, Youqing Shen, Hailin Cong, (2019, Dec.). "Photocatalytic potential of bio-engineered copper nanoparticles synthesized from Ficus carica extract for the degradation of toxic organic dye from waste water: Growth mechanism and study of parameter affecting the degradation performance", *Materials Research Bulletin*. 120, pp. 110583. Available: https://doi.org/10.1016/j.materresbull.2019.110583

[6] Subramanian Natarajan, Hari C. Bajaj, Rajesh J. Tayade, (2018, Mar.). "Recent advances based on the synergetic effect of adsorption for removal of dyes from waste water using photocatalytic process", *Journal of Environmental Sciences*. 65, pp. 201-222. Available: https://doi.org/10.1016/j.jes.2017.03.011.

[7] K. Meghana Navada, Nagaraja G. K, Ranjitha R, Josline Neetha D'Souza, Sabia Kouser & Manasa D. J, (2021, Mar.). "Synthesis, characterization of phyto-functionalized CuO nano photocatalysts for mitigation of textile dyes in waste water purification, antioxidant, anti-inflammatory and anticancer evaluation", *Applied Nanoscience.* 11, pp. 1313–1338. Available: https://doi.org/10.1007/s13204-021-01688-9.

[8] E. Nyankson, R.V. Kumar, (2019, Dec.). "Removal of water-soluble dyes and pharmaceutical wastes by combining the photocatalytic properties of Ag_3PO_4 with the adsorption properties of halloysite nanotubes", *Materialstoday Advances.* 4, pp. 100025. Available: https://doi.org/10.1016/j.mtadv.2019.100025.

[9] John Bani Fathima, Arivalagan Pugazhendhi, Mohammad Oves, Rose Venis, (2018, Jan.). "Synthesis of eco-friendly copper nanoparticles for augmentation of catalytic degradation of organic dyes", *Journal of Molecular Liquids.* 260, pp. 1-8 Available: https://doi.org/10.1016/j.molliq.2018.03.033.

[10] Sushmita Banerjee, M.C. Chattopadhyaya, (2017, May). "Adsorption characteristics for the removal of a toxic dye, tartrazine from aqueous solutions by a low cost agricultural by-product", *Arabian Journal of Chemistry.* 10(2), pp. S1629-S1638 Available: https://doi.org/10.1016/j.arabjc.2013.06.005.

[11] Q. Zheng, D.P. Durkin, J.E. Elenewski, Y. Sun, N.A. Banek, L. Hua, H. Chen, M. J. Wagner, W. Zhang, D. Shuai, (2016, Nov.). "Visible-Light-Responsive Graphitic Carbon Nitride: Rational Design and Photocatalytic Applications for Water Treatment", *Environmental Science & Technology.* 50(23). Available: https://doi.org/10.1021/acs.est.6b02579.

[12] H. Wang, Y. Wu, M. Feng, W. Tu, T. Xiao, T. Xiong, H. Ang, X. Yuan, J.W. Chew, (2018, Nov.). "Visible-light-driven removal of tetracycline antibiotics and reclamation of hydrogen energy from natural water matrices and wastewater by polymeric carbon nitride foam", *Water Research. 144*, pp. 215-225. Available: https://doi.org/10.1016/j.watres.2018.07.025.

[13] C.C. Wang, J.R. Li, X.L. Lv, Y.Q. Zhang, (2014, Jul.). "Visible-light-driven removal of tetracycline antibiotics and reclamation of hydrogen energy from natural water matrices and wastewater by polymeric carbon nitride foam", *Energy Environ. Sci. 7*, pp. 2831-2867. Available: https://doi.org/10.1039/C4EE01299B.

[14] D-T. Tran, T-H. Nguyen, T-P-T. Vu, V-Q. Dang, T-T-T. Le, H-T. Van, (2024, Jan.). "Photocatalytic organic pollutants degradation in metal–organic frameworks", *Journal of Water Process Engineering. 57*, pp. 104687. Available: https://doi.org/10.1039/C4EE01299B.

[15] T. T. T. Le, T. L. Nguyen, D-T. Tran and V. N. Nguyen, (2019, Jun.). "Enhanced Photocatalytic Degradation of Rhodamine B Using C/Fe Co-Doped Titanium Dioxide Coated on Activated Carbon", *Journal of Chemistry.* pp. 2949316. Available: https://doi.org/10.1155/2019/2949316.

[16] D-T. Tran, T-H. Ha, T-P-T. Vu, V-N. Nguyen, T-D. Pham, (2024, Mar.). "Novel CeO_2-V_2O_5/rGO tertiary photocatalyst for improved cefotaxime degradation using visible-light", *Inorganic Chemistry Communications. 161,* pp. 112044. Available: https://doi.org/10.1016/j.inoche.2024.112044.

[17] H.B. Hadjltaief, S.B. Ameur, P. D. Costa, M.B. Zina, M.E. Galvez, (2018, Feb.). "Photocatalytic decolorization of cationic and anionic dyes over ZnO nanoparticle immobilized on natural Tunisian clay", *Applied Clay Science. 152*, pp. 148-157. Available: https://doi.org/10.1016/j.clay.2017.11.008.

[18] D. S. Manu & Arun Kumar Thalla, (2018, Jan.). "Influence of various operating conditions on wastewater treatment in an AS-biofilm reactor and post-treatment using TiO_2-based solar/UV photocatalysis", *Environmental Technology. 40*, pp. 1271–1288. Available: https://doi.org/10.1080/09593330.2017.1420697.

[19] I. Jellal, K. Nouneh, J. Jedryka, D. Chaumont, J. Naja, (2020, Oct.). "Non-linear optical study of hierarchical 3D Al doped ZnO nanosheet arrays deposited by successive ionic adsorption and reaction method", *Optics & Laser Technology. 130*, pp. 106348. Available: https://doi.org/10.1016/j.optlastec.2020.106348.

[20] R. Ebrahimi, K. Hossienzadeh, A. Maleki, R. Ghanbari, R. Rezaee, M. Safari, B. Shahmoradi, H. Daraei, A. Jafari, K. Yetilmezsoy, S.H. Puttaiah, (2019, April.). "Effects of doping zinc oxide nanoparticles with transition metals (Ag, Cu, Mn) on photocatalytic degradation of Direct Blue 15 dye under UV and visible light irradiation", *Journal of Environmental Health Science and Engineering. 17*, pp. 479–492. Available: https://doi.org/10.1007/s40201-019-00366-x.

[21] J.C. Murillo-Sierra, A. Hernández-Ramírez, L. Hinojosa-Reyes, J.L. Guzmán-Mar, (2021, Mar.). "A review on the development of visible light-responsive WO_3-based photocatalysts for environmental applications", *Chemical Engineering Journal Advances. 5*, pp. 100070. Available: https://doi.org/10.1016/j.ceja.2020.100070.

[22] I.M. Szilagyi, B. Forizs, O. Rosseler, A. Szegedi, P. Nemeth, P. Kiraly, G. Tarkanyi, B. Vajna, K. Varga-Josepovits, K. Laszlo, A.L. Tóth, P. Baranyai, M. Leskelä, (2012, Oct.). "WO_3 photocatalysts: Influence of structure and composition", *Journal of Catalysis. 294*, pp. 119-127. Available: https://doi.org/10.1016/j.jcat.2012.07.013.

[23] Y. Liu, Y. Li, W. Li, S. Han, C. Liu, (2012, April.). "Photoelectrochemical properties and photocatalytic activity of nitrogen-doped nanoporous WO_3 photoelectrodes under visible light", *Applied Surface Science*. 258 (12), pp. 5038-5045. Available: https://doi.org/10.1016/j.apsusc.2012.01.080.

[24] F. Mehmood, J. Iqbal, M. Ismail, A. Mehmood, (2018, May). "Ni doped WO_3 nanoplates: An excellent photocatalyst and novel nanomaterial for enhanced anticancer activities", *Journal of Alloys and Compounds*. 746, pp. 729-738. Available: https://doi.org/10.1016/j.jallcom.2018.01.409.

[25] J. Chen, X. Xiao, Y. Wang, Z. Ye, J., (2019, Mar.). "Fabrication of hierarchical sheet-on-sheet WO_3/g-C_3N_4 composites with enhanced photocatalytic activity", *Journal of Alloys and Compounds*. 777, pp. 325-334. Available: https://doi.org/10.1016/j.jallcom.2018.10.404.

[26] V. Ramar, K. Balasubramanian, (2021, May). "Reduced Graphene Oxide/WO_3 Nanorod Composites for Photocatalytic Degradation of Methylene Blue under Sunlight Irradiation", *ACS Applied Nano Materials*. 4(5). Available: https://doi.org/10.1021/acsanm.1c00863.

[27] M.G. Peleyeju, E.L. Viljoen, J., (2021, April.). "WO_3-based catalysts for photocatalytic and photoelectrocatalytic removal of organic pollutants from water - A review", *Journal of Water Process Engineering*. 40, pp. 101930. Available: https://doi.org/10.1016/j.jwpe.2021.101930.

[28] Q. Zhu, S. Xu, Y. Qin, J.C.-H. Lam, Y. Li, (2022, Nov.). "Multication and Structure Regulation: Utilizing X-Doped (X = Co, Mn, Cu) ZnS/CoO Hollow Composites to Spatially Propel the Charge for Superior Solar Hydrogen Evolution", *Solar*. 40, pp. 101930. Available: https://doi.org/10.1002/solr.202200918.

[29] Y. Fan, C. He, Y. Li, (2022, Aug.). "Iron oxide clusters on g-C_3N_4 promote the electron–hole separation in photo-Fenton reaction for efficient degradation of wastewater", *Chemical Papers*. 76, pp. 7553–7563. Available: https://doi.org/10.1007/s11696-022-02419-2.

[30] M. Liao, L. Su, Y. Deng, S. Xiong, R. Tang, Z. Wu, C. Ding, L. Yang, D. Gong, (2021, Jun.). "Strategies to improve WO_3-based photocatalysts for wastewater treatment: a review", *Journal of Materials Science*. 56, pp. 14416–14447. Available: https://doi.org/10.1007/s10853-021-06202-8.

[31] T.P.T. Vu, D.T. Tran, V.C. Dang, (2022, Mar.). "Novel N,C,S-TiO_2/WO_3/rGO Z-scheme heterojunction with enhanced visible-light driven photocatalytic performance", *Journal of Colloid and Interface Science*. 610, pp. 49-60.

[32] V. N. Nguyen, D-T. Tran, M. T. Nguyen, T. T. T. Le, M. N. Ha, M. V. Nguyen & T-D. Pham, (2018, Jan.). "Enhanced photocatalytic degradation of methyl orange using ZnO/graphene oxide nanocomposites", *Research on Chemical Intermediates.* 44, pp. 3081–3095. Available: https://doi.org/10.1007/s11164-018-3294-3.

[33] V. N. Kalpana, B.A.S. Kataru, N. Sravani, T. Vigneshwari, A. Panneerselvam, V. Devi Rajeswari, (2018). "Biosynthesis of zinc oxide nanoparticles using culture filtrates of Aspergillus niger: Antimicrobial textiles and dye degradation studies", *Open Nano.* 3, pp. 48-55. Available: https://doi.org/10.1016/j.onano.2018.06.001.

[34] S. Talam, S.R. Karumuri, N. Gunnam, (2012, May.). "Synthesis, Characterization, and Spectroscopic Properties of ZnO Nanoparticles", *ISRN*. Available: https://doi.org/10.5402/2012/372505.

[35] M-C. Le, V-T. Hoang, X-K. Bui, V-T. Pham, C-T. Nguyen, T-L-A. Luu & D-T. Tran, (2023, Mar). "Synthesis of g-C_3N_4@WO_3 nanocomposites for dye adsorptive removal in water medium: Equilibrium and kinetics studies", *Journal of Dispersion Science and Technology*. 45(9), pp. 1733-1745. Available: https://doi.org/10.1080/01932691.2023.2228892.

[36] Q. Hao, T. Liu, J. Liu, Q. Liu, X. Jing, H. Zhang, G. Huang, J. Wang, (2017, Mar). "Controllable synthesis and enhanced gas sensing properties of a single-crystalline WO_3–rGO porous nanocomposite", *RSC Adv.* 7, pp. 14192-14199. Available: https://doi.org/10.1039/C6RA28379A.

[37] J. Zhang, Z. Peng, A. Soni, Y. Zhao, Y. Xiong, (2011, May). "Raman Spectroscopy of Few-Quintuple Layer Topological Insulator Bi_2Se_3 Nanoplatelets", *Nano Letters.* 11(6), pp. 2407–2414. Available: https://doi.org/10.1021/nl200773n.

[38] R. C. Ngullie, S.O. Alaswad, K. Bhuvaneswari, P. Shanmugam, T. Pazhanivel, P. Arunachalam, (2020, May). "Synthesis and Characterization of Efficient ZnO/g-C_3N_4 Nanocomposites Photocatalyst for Photocatalytic Degradation of Methylene Blue", *Coatings.* 10(5), pp. 500. Available: https://doi.org/10.3390/coatings10050500.

[39] Z. Zaidi, S.I. Siddiqui, B. Fatima, S.A. Chaudhry, (2019, Dec). "Synthesis of ZnO nanospheres for water treatment through adsorption and photocatalytic degradation: Modelling and process optimization", *Materials Research Bulletin.* 120, pp. 110584. Available: https://doi.org/10.1016/j.materresbull.2019.110584.

[40] Thu-Hien Le, Dinh-Trinh Tran, Thi-Phuong-Thao Vu, Long D. Nghiem, (2023, Sep.). "A novel tertiary magnetic $ZnFe_2O_4$/BiOBr/rGO nanocomposite catalyst for photodegrading organic contaminants by visible light", *Science of The Total*

Environment. 891, pp. 164358. Available: https://doi.org/10.1016/j.scitotenv.2023.164358.

[41] V. Hasija, P. Raizada, A. Sudhaik, P. Singh, V.K. Thakur, A. A. P. Khan, (2020, Feb.). "Fabrication of Ag/AgI/WO_3 heterojunction anchored P and S co-doped graphitic carbon nitride as a dual Z scheme photocatalyst for efficient dye degradation", *Solid State Sciences.* 100, pp. 106095. Available: https://doi.org/10.1016/j.solidstatesciences.2019.106095.

[42] M. Verma, K. P. Singh, A. Kumar, (2020, Jan.). "Reactive magnetron sputtering based synthesis of WO_3 nanoparticles and their use for the photocatalytic degradation of dyes", *Solid State Sciences.* 99, pp. 105847. Available: https://doi.org/10.1016/j.solidstatesciences.2019.02.008.

[43] Thi Thanh Thuy Le, Dinh Trinh Tran, Thi Huong Danh, (2021, May.). "Remarkable enhancement of visible light driven photocatalytic performance of TiO_2 by simultaneously doping with C, N, and S", *Chemical Physics.* 545, pp. 111144. Available: https://doi.org/10.1016/j.chemphys.2021.111144.

[44] Thuy Thi Thanh Le, Trinh Dinh Tran, (2020, Jul.). "Photocatalytic Degradation of Rhodamine B by C and N Codoped TiO_2 Nanoparticles under Visible-Light Irradiation", *Journal of chemistry.* Available: https://doi.org/10.1155/2020/4310513.

[45] Linyan Zhao, Xiaoli Xi, Yangsi Liu, Liwen Ma, Zuoren Nie, (2020, Jan.). "Facile synthesis of WO_3 micro/nanostructures by paper-assisted calcination for visible-light-driven photocatalysis", *Chemical Physics.* 528, pp. 110515. Available: https://doi.org/10.1016/j.chemphys.2019.110515.

[46] X. Wang, X. Wang, H. Yang, A. Meng, Z. Li, L. Yang, L. Wang, S. Li, G. Li, J. Huang, (2022, Mar.). "Interfacial engineering improved internal electric field contributing to direct Z-scheme-dominated mechanism over CdSe/SL-$ZnIn_2S_4$/$MoSe_2$ heterojunction for efficient photocatalytic hydrogen evolution", *Chemical Engineering Journal.* 431, pp. 134000. Available: https://doi.org/10.1016/j.cej.2021.134000.

[47] H. F. Moafi, M. A. Zanjanchi, A.F. Shojaie, (2013, May). "Tungsten-doped ZnO nanocomposite: Synthesis, characterization, and highly active photocatalyst toward dye photodegradation", *Materials Chemistry and Physics.* 139 (2-3), pp. 856-864. Available: https://doi.org/10.1016/j.matchemphys.2013.02.044.

[48] J. Hasan, H. Li, G. Tian, C. Qin, (2020, Nov.). "Fabrication of Cr_2S_3-GO-TiO_2 composite with high visible-light-driven photocatalytic activity on degradation of organic dyes", *Chemical Physics.* 539, pp. 110950. Available: https://doi.org/10.1016/j.chemphys.2020.110950.

[49] Thi-Phuong-Thao Vu, Dinh-Trinh Tran, Quang-Trung Pham, (2022, Dec.). "Novel CdS/MIL-88A heterojunction coupled with H_2O_2/air-nanobubbles for enhanced visible-light driven photocatalytic performance", *Journal of Cleaner Production.* 380, pp. 135007. Available: https://doi.org/10.1016/j.jclepro.2022.135007.

[50] M. Kumar, R. Vaish, S. ben Ahmed, (2021, Nov.). "Piezo-photocatalytic activity of mechanochemically synthesized $BiVO_4$ for dye cleaning", *J. Am Ceram Soc.* pp. 18233. Available: https://doi.org/10.1111/jace.18233.

[51] Y. Subramanian, V. Ramasamy, R.J. Karthikeyan, G.R. Srinivasan, D. Arulmozhi, R.K. Gubendiran, M. Sriramalu, (2019, Jun.). "Investigations on the enhanced dye degradation activity of heterogeneous $BiFeO_3$–$GdFeO_3$ nanocomposite photocatalyst", *Journal of Cleaner Production.* 5(6), pp. e01831. Available: https://doi.org/10.1016/j.heliyon.2019.e01831.

[52] Geng Yanling, Li Na, Ma Jiyan, Sun Zhenhai, (2017, May.). "Preparation, characterization and photocatalytic properties of BiOBr/ZnO composites", *Journal of Energy Chemistry.* 26(3), pp. e01831. Available: https://doi.org/10.1016/j.jechem.2017.01.002.

[53] E. Benavente, F. Durán, C. Sotomayor-Torres, G. González, (2018, Feb.). "Heterostructured layered hybrid ZnO/MoS_2 nanosheets with enhanced visible light photocatalytic activity", *Journal of Physics and Chemistry of Solids*, pp. 119-124. Available: https://doi.org/10.1016/j.jpcs.2017.10.027.

[54] S. Alkaykh, A. Mbarek, E.E. Ali-Shattle, (2018, Feb.). "Photocatalytic degradation of methylene blue dye in aqueous solution by $MnTiO_3$ nanoparticles under sunlight irradiation", *Heliyon.* 6(4), pp. e03663. Available: https://doi.org/10.1016/j.heliyon.2020.e03663.

[55] N. K.A. Hamed, M.K. Ahmad, N.H.H. Hairom, A.B. Faridah, M.H. Mamat, A. Mohamed, A.B. Suriani, C.F. Soon, F.I.M. Fazli, S.M. Mokhtar, M. Shimomura, (2022, Jan.). "Photocatalytic degradation of methylene blue by flowerlike rutile-phase TiO_2 film grown via hydrothermal method", *Journal of Sol-Gel Science and Technology.*102, pp. 637–648. Available: https://doi.org/10.1007/s10971-021-05691-y.

[56] N. K.A. Hamed, M.K. Ahmad, N.H.H. Hairom, A.B. Faridah, M.H. Mamat, A. Mohamed, A.B. Suriani, C.F. Soon, F.I.M. Fazli, S.M. Mokhtar, M. Shimomura, (2022, Nov.). "Piezo-photocatalytic activity of $Bi_2VO_{5.5}$ for methylene blue dye degradation", *Journal of Materials Research and Technology*. 21, pp. 1998-2012. Available: https://doi.org/10.1016/j.jmrt.2022.09.130.

[57] T.T.T. Nguyen, S.D. Dao, V.T. Doan, T.A. Tahtamouni, T-D. Pham, T.H. Nguyen, D-T. Tran, M-V. Nguyen, N-M. Dang, T.P.L.C. Nguyen, V.N. Nguyen, (2019, Sep.). "Piezo-photocatalytic activity of $Bi_2VO_{5.5}$ for methylene blue dye degradation", *Applied Surface Science.* 489, pp. 875-882. Available: https://doi.org/10.1016/j.apsusc.2019.05.360.

[58] B.D. Ngom, O. Sakho, N. Manyala, J.B. Kana, N. Mlungisi, L. Guerbous, A.Y. Fasasi, M. Maaza, A.C. Beye, (2009, May.). "Structural, morphological and photoluminescence properties of W-doped ZnO nanostructures", *Applied Surface Science.* 255(16), pp. 7314-7318. Available: https://doi.org/10.1016/j.apsusc.2009.03.089.

Ngày nhận bài: 24/12/2024 Ngày chấp nhận đăng: 21/3/2025